Supplementary Information

Understanding divergent Brown Carbon Photobleaching Rates from Molecular Perspective

Yanting Qiu[1], Tao Qiu[2], Yuechen Liu[3], Yu Gu[2], Ruiqi Man[1], Dapeng Liang[2], Taomou Zong[1], Zhijun Wu[1,4,], Min Hu[1]*

1 State Key Laboratory of Regional Environment and Sustainability, College of Environmental Sciences and Engineering, Peking University, Beijing 100871, China

2 Key Lab of Groundwater Resources and Environment of the Ministry of Education, College of New Energy and Environment, Jilin University, Changchun 130012, China

3 National Institute of Metrology, Beijing 100029, China

4 Collaborative Innovation Center of Atmospheric Environment and Equipment Technology, Nanjing University of Information Science and Technology, 210044, Nanjing, China

*Correspondence Author:

Zhijun Wu (zhijunwu@pku.edu.cn)

Text S1

Tables S1-S6

Figures S1-S6

Text S1 The measurement of steady-state OH radical concentration

The steady-state OH radical concentration ($[OH]_{ss}$) was measured using the peudo-first order decay of benzoic acid (BA, 98%, Alaadin Inc.). According to previous study (Hems and Abbatt, 2018), BA had a secondary order rate constant with OH radicals. The peudo-first order decay of BA, the relationship between the peudo-first order rate constant and secondary order rate constant respectively followed eq.(S1) and eq.(S2).

$$BA_t = BA_0 \times \exp(-k_{BA}^{I} t) \quad \text{(S1)}$$

$$k_{BA}^{I} = k_{BA}^{II} \times [OH]_{ss} \quad \text{(S2)}$$

In eqs.(S1), the BA_t and BA_0 was the concentration of BA after t hours of equivalent solar radiation and before photochemical aging, respectively. We conducted a series of parallel experiments to measure the $[OH]_{ss}$, i.e., samples from this set of experiments were only used to analyze the variations in the concentration of BA and not for other analysis. The secondary order rate constant for BA (k_{BA}^{II}) was 2.1×10^{13} M^{-1} h^{-1}. In this work, the measured $[OH]_{ss}$ was $(3.17 \pm 0.47) \times 10^{-14}$ M.

Table S1 The concentrations of OC, EC, and TOC of each biomass burning $PM_{2.5}$ sample

Sample	OC (μg/m^3)	EC (μg/m^3)	TOC (μg/m^3)
Corn Straw-1	1900.29	1835.05	830.60
Corn Straw-2	1997.20	1539.04	704.54
Corn Straw-3	1348.73	1006.39	753.89
Corn Straw-4	1890.32	1582.93	854.89

Table S2 The average mass concentration of $PM_{2.5}$, concentration of gaseous pollutants, ambient RH, and chemical composition in NR-PM_1 during the sampling period of $PM_{2.5}$ filters for the isolation of BrC

species (unit)	average (± standard deviation)
$PM_{2.5}$ (μg/m^3)	53.46 (± 20.97)
O_3 (ppb)	10.94 (± 9.27)
SO_2 (ppb)	1.36 (± 1.17)
CO (ppm)	0.72 (± 0.31)
NO_2 (ppb)	24.77 (± 12.34)
RH (%)	43.21 (± 19.58)
sulfate (μg/m^3)	3.79 (± 2.57)
nitrate (μg/m^3)	11.33 (± 7.65)
organics (μg/m^3)	12.64 (± 6.64)

Table S3 The MAC, calculated k_{BrC}, and corresponding references of Figure 1(b) in the main text

BrC Type	MAC ($cm^2\ g^{-1}$)	k_{BrC} (h^{-1})	Reference
aq-BrC	7548.68	1.13	this work
p-BrC	787.66	0.10	
b-BrC	9340.82	0.05	
aq-BrC	6300	4.02	(Müller et al., 2023)
SRFA	32000	0.007	
b-BrC	10000	0.07	
p-BrC	400	0.08	
b-BrC	6400	0.05	(Hems et al., 2020)
4-nitrocatechol	12000	0.04	(Hems and Abbatt, 2018)
aq-BrC	4200	6.60	(Aiona et al., 2017)
Limonene-O_3-SOA	800	2.28	
CDOM	26000	0.02	(Borduas-Dedekind et al., 2019)
b-BrC	7000	0.07	(Fleming et al., 2020)
b-BrC	6300	0.04	(Wong et al., 2019)
p-BrC	650	0.08	(Qiu et al., 2024)
2,4-dinitrophenol	11000	0.05	(Liu et al., 2025)
3-nitrocatechol	10000	0.04	
Wood smoke SOA	8000	0.18	(Liu-Kang et al., 2022)
b-BrC	7600	0.20	(Choudhary et al., 2023)
b-BrC	14000	0.02	(Fan et al., 2020)
aq-BrC	2200	0.85	(Gao and Zhang, 2019)

Table S4 Detected products after photochemical aging for aq-BrC

m/z	elemental composition	chemical structure	MS^2 fragments
99.01	$C_4H_4O_3$	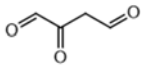	-*
113.02	$C_5H_6O_3$	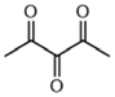	95, 61
125.04	$C_5H_6O_2N_2$	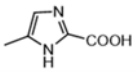	81, 72
139.05	$C_6H_8O_2N_2$	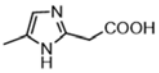	95, 69, 59
167.05	$C_7H_8O_3N_2$	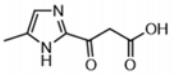	123, 59
180.05	$C_8H_9O_3N_2$	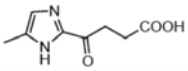	137, 109, 81
189.08	$C_8H_{14}O_5$	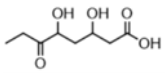	115, 71, 59
195.08	$C_9H_{12}O_3N_2$	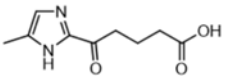	151, 123, 97, 81
213.08	$C_{10}H_{14}O_5$	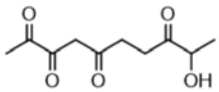	195, 127, 85

*: The MS^2 fragments were not available due to low signal intensities of parent ions or the *m/z* of MS^2 fragments were below the lower limit of instrument

Table S5 Detected products after photochemical aging for p-BrC

m/z	elemental composition	chemical structure	MS^2 fragments
111.01	$C_5H_4O_3$	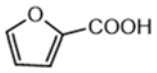	67
115.00	$C_4H_4O_4$	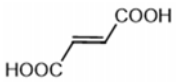	71, 68
141.03	$C_5H_6O_3N_2$	-	-
165.02	$C_8H_6O_4$	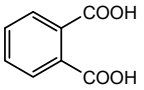	93
166.05	$C_8H_9NO_3$	-	-
168.98	$C_3H_6O_6S$	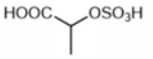	125, 97
182.01	$C_7H_5NO_5$	-	-
186.00	$C_6H_5O_6N$	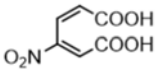	141, 124, 95
190.04	$C_6H_9O_6N$	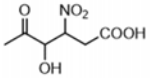	145, 99
202.00	$C_6H_5O_7N$	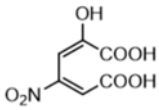	158, 141, 130
208.06	$C_{10}H_{11}NO_4$	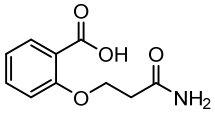	137, 93
217.99	$C_6H_5O_8N$	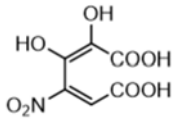	173, 127, 100, 72
233.99	$C_6H_5O_9N$	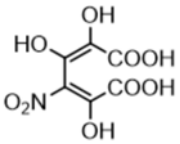	189, 144, 116, 73
240.05	$C_{10}H_{11}O_6N$	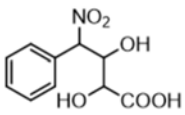	195, 162, 149

Table S5 Continued

m/z	elemental composition	chemical structure	MS^2 fragments
246.02	$C_8H_9O_8N$	-	201, 130, 114, 69
248.03	$C_7H_{11}O_5N_3S$	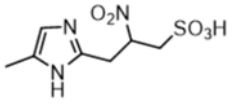	153, 136, 81

Table S6 Detected products after photochemical aging for b-BrC

m/z	elemental composition	chemical structure	MS^2 fragments
111.01	$C_5H_4O_3$	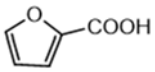	67
149.02	$C_8H_6O_3$	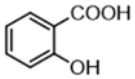	93, 65
165.02	$C_8H_6O_4$	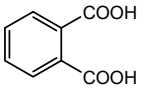	93
166.05	$C_8H_9O_3N$	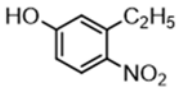	-
183.04	$C_{12}H_8O_2$	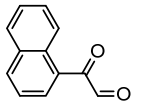	127, 101, 77
186.00	$C_6H_5O_6N$	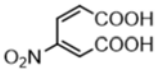	141, 124, 95
190.04	$C_6H_9O_6N$	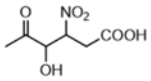	145, 99
202.00	$C_6H_5O_7N$	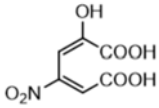	158, 141, 130
208.06	$C_{10}H_{11}NO_4$	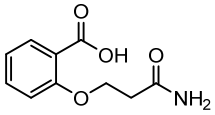	137, 93
217.99	$C_6H_5O_8N$	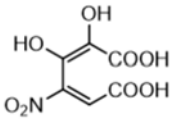	173, 127, 100, 72
225.09	$C_{15}H_{14}O_2$	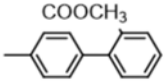	193, 167, 141
233.99	$C_6H_5O_9N$	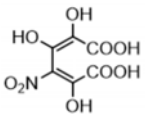	189, 144, 116, 73

Table S6 Continued

m/z	elemental composition	chemical structure	MS^2 fragments
244.03	$C_8H_9O_7N_2$	-	-
335.05	$C_{14}H_{12}N_2O_8$	-	-
391.08	$C_{15}H_{16}O_5N_6S$	-	-

Figure S1 Typical sample collection process of biomass burning $PM_{2.5}$ samples

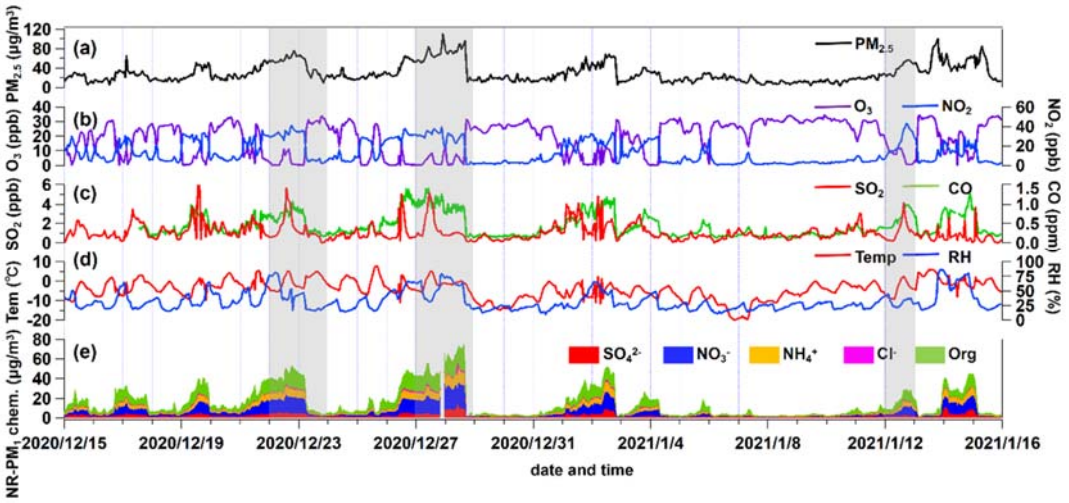

Figure S2 Time series of gaseous pollutants concentrations, $PM_{2.5}$ mass concentrations, chemical composition of NR-PM_1, and meteorological parameters during the field observation.

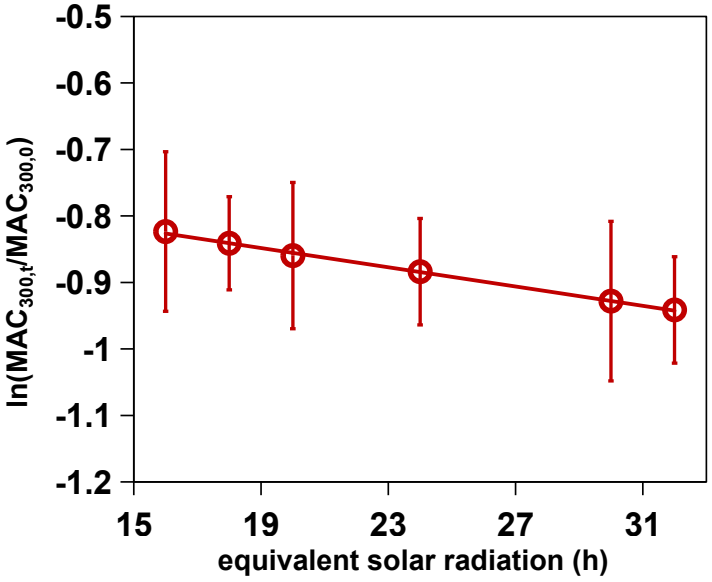

63

64 **Figure S3** The variations in ln($MAC_{300,t}/MAC_{300,0}$) of b-BrC when the equivalent solar radiation
65 was expanded to 32 h

66

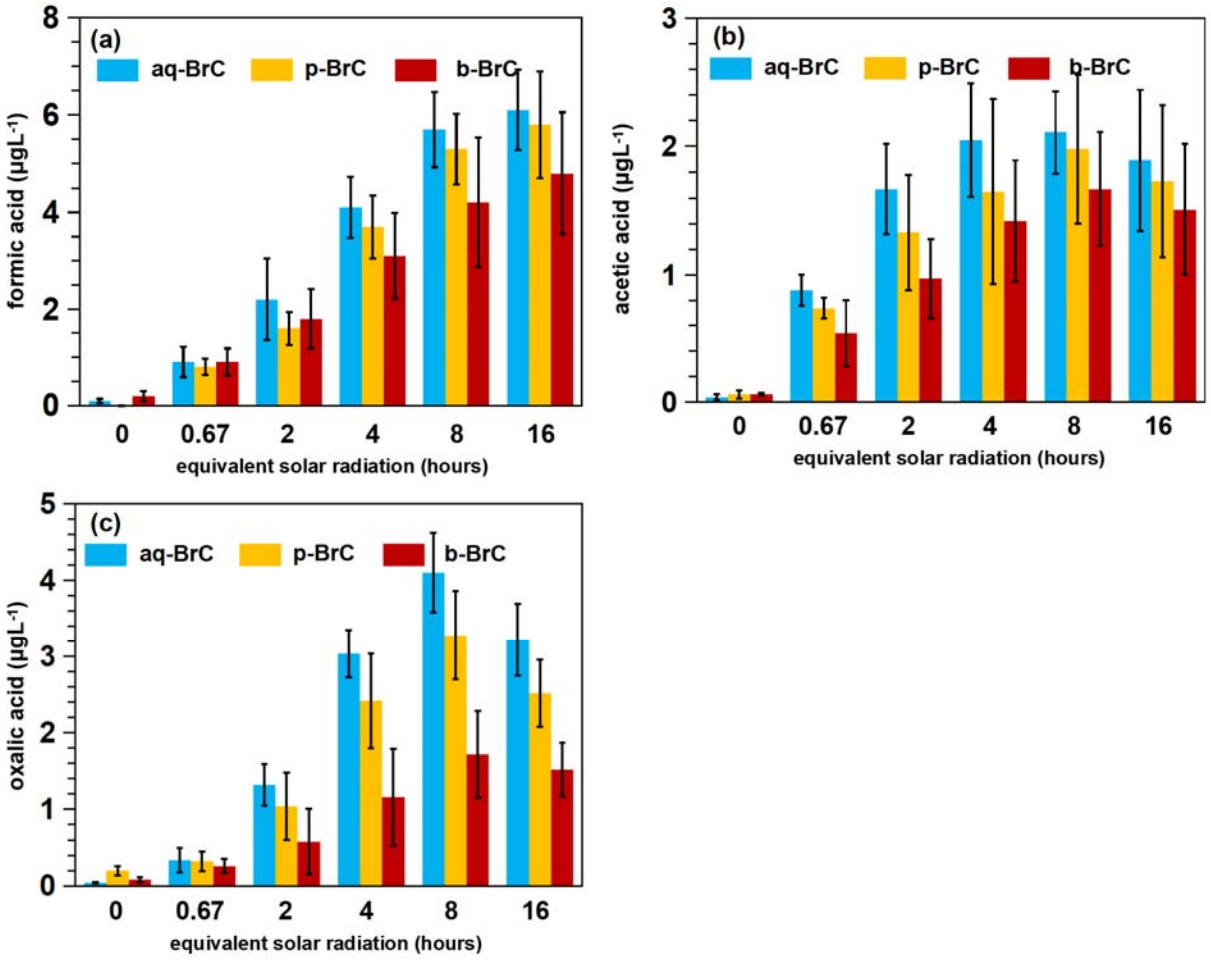

Figure S4 The variations in (a) formic acid, (b) acetic acid, and (c) oxalic acid as a function of equivalent solar radiation hours. The legend was shared in all panels.

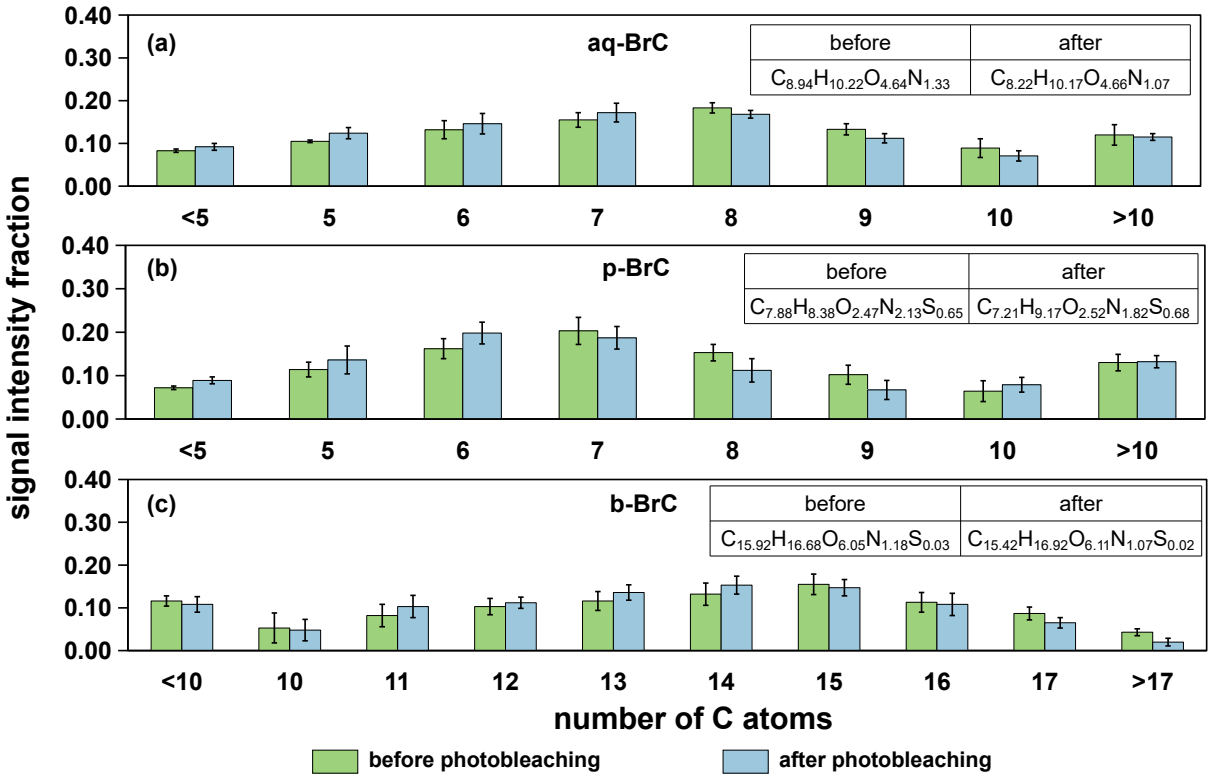

Figure S5 The signal intensity fraction distributions of detected compounds with different number of C atoms before and after photobleaching for (a) aq-BrC, (b) p-BrC, and (c) b-BrC. Error bars represent one standard deviation of datapoints derive from three (aq-BrC and b-BrC) or five (p-BrC) parallel experiments. The inserted tables are signal-intensity-weighted average elemental composition of BrC.

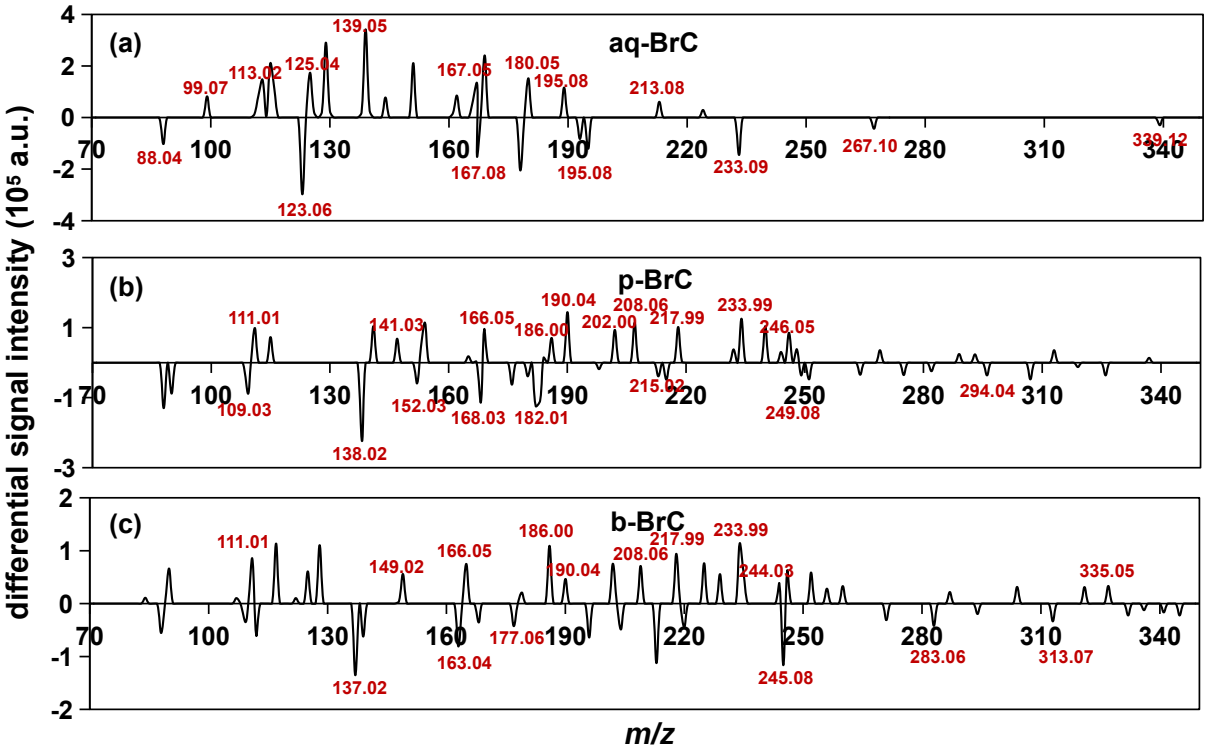

Figure S6 The differential HRMS spectra of (a) aq-BrC, (b) p-BrC, and (c) b-BrC before and after photobleaching. The positive and negative peaks respectively represent signal intensities increase and decrease after photobleaching.

SI References

Aiona, P. K., Lee, H. J., Leslie, R., Lin, P., Laskin, A., Laskin, J., Nizkorodov, S. A.: Photochemistry of Products of the Aqueous Reaction of Methylglyoxal with Ammonium Sulfate. ACS Earth and Space Chemistry. 1, 522-532. 10.1021/acsearthspacechem.7b00075, 2017.

Borduas-Dedekind, N., Ossola, R., David, R. O., Boynton, L. S., Weichlinger, V., Kanji, Z. A., McNeill, K.: Photomineralization mechanism changes the ability of dissolved organic matter to activate cloud droplets and to nucleate ice crystals. Atmospheric Chemistry and Physics. 19, 12397-12412. 10.5194/acp-19-12397-2019, 2019.

Choudhary, V., Roson, M. L., Guo, X., Gautam, T., Gupta, T., Zhao, R.: Aqueous-phase photochemical oxidation of water-soluble brown carbon aerosols arising from solid biomass fuel burning. Environmental Science: Atmospheres. 3, 816-829. 10.1039/D2EA00151A, 2023.

Fan, X., Cao, T., Yu, X., Wang, Y., Xiao, X., Li, F., Xie, Y., Ji, W., Song, J., Peng, P.: The evolutionary behavior of chromophoric brown carbon during ozone aging of fine particles from biomass burning. Atmospheric Chemistry and Physics. 20, 4593-4605. 10.5194/acp-20-4593-2020, 2020.

Fleming, L. T., Lin, P., Roberts, J. M., Selimovic, V., Yokelson, R., Laskin, J., Laskin, A., Nizkorodov, S. A.: Molecular composition and photochemical lifetimes of brown carbon chromophores in biomass burning organic aerosol. Atmospheric Chemistry and Physics. 20, 1105-1129. 10.5194/acp-20-1105-2020, 2020.

Gao, Y., Zhang, Y.: Optical properties investigation of the reactions between methylglyoxal and glycine/ammonium sulfate. Spectrochimica Acta Part A: Molecular and Biomolecular Spectroscopy. 215, 112-121. https://doi.org/10.1016/j.saa.2019.02.087, 2019.

Hems, R. F., Abbatt, J. P. D.: Aqueous Phase Photo-oxidation of Brown Carbon Nitrophenols: Reaction Kinetics, Mechanism, and Evolution of Light Absorption. ACS Earth and Space Chemistry. 2, 225-234. 10.1021/acsearthspacechem.7b00123, 2018.

Hems, R. F., Schnitzler, E. G., Bastawrous, M., Soong, R., Simpson, A. J., Abbatt, J. P. D.: Aqueous Photoreactions of Wood Smoke Brown Carbon. ACS Earth and Space Chemistry. 4, 1149-1160. 10.1021/acsearthspacechem.0c00117, 2020.

Liu-Kang, C., Gallimore, P. J., Liu, T., Abbatt, J. P. D.: Photoreaction of biomass burning brown carbon aerosol particles. Environmental Science: Atmospheres. 2, 270-278. 10.1039/d1ea00088h, 2022.

Liu, Y., Huang, R.-J., Lin, C., Yuan, W., Li, Y. J., Zhong, H., Yang, L., Wang, T., Huang, W., Xu, W., Huang, D. D., Huang, C.: Nitrate-Photolysis Shortens the Lifetimes of Brown Carbon Tracers from Biomass Burning. Environmental Science & Technology. 59, 640-649. 10.1021/acs.est.4c06123, 2025.

Müller, S., Giorio, C., Borduas-Dedekind, N.: Tracking the Photomineralization Mechanism in Irradiated Lab-Generated and Field-Collected Brown Carbon Samples and Its Effect on Cloud Condensation Nuclei Abilities. ACS Environmental Au. 3, 164-178. 10.1021/acsenvironau.2c00055, 2023.

Qiu, Y., Qiu, T., Wu, Z., Liu, Y., Fang, W., Man, R., Liu, Y., Wang, J., Meng, X., Chen, J., Liang, D., Guo, S., Hu, M.: Observational Evidence of Brown Carbon Photobleaching in Urban Atmosphere at Molecular Level. Environmental Science and Technology Letters. 11, 1032-1039. 10.1021/acs.estlett.4c00647, 2024.

Wong, J. P. S., Tsagkaraki, M., Tsiodra, I., Mihalopoulos, N., Violaki, K., Kanakidou, M., Sciare, J., Nenes, A., Weber, R. J.: Atmospheric evolution of molecular-weight-separated brown carbon from biomass burning. Atmospheric Chemistry and Physics. 19, 7319-7334. 10.5194/acp-19-7319-2019, 2019.